Univerzita Komenského v Bratislave

Fakulta matematiky, fyziky a informatiky

Riyas Subair

Autoreferát dizertačnej práce

Fotovoltaické perovskitové štruktúry dopované s nanobodkami a ich stabilita

na získanie akademického titulu philosophiae doctor

v odbore doktorandského štúdia:
4.1.4. Kvantová elektronika a optika

Miesto a dátum:
Bratislava, 2020

Dizertačná práca bola vypracovaná v dennej forme doktorandského štúdia

na Fyzikálnom ústave Slovenskej akadémie vied

Predkladateľ: **Mgr. Riyas Subair**
Fyzikálny ústav SAV
Dúbravská cesta 9
845 11 Bratislava

Školiteľ: **RNDr. Eva Majkova, DrSc.**
Fyzikálny ústav SAV

4.1.4. Kvantová elektronika a optika

Predseda odborovej komisie:

.....
(meno a priezvisko s uvedením titulov a hodností
a presná adresa jeho zamestnávateľa)

Abstrakt

Perovskitové solárne články (PSCs) zaznamenali za posledných 10 rokov excelentný nárast účinnosti konverzie PCE od 9% až do 25%. PSCs sú multivrstvová štruktúra, v ktorej je aktívna vrstva perovskitu obklopená vrstvami pre selektívny transport náboja k elektródam. Štruktúra, morfológia a transportné vlastnosti vrstiev a rozhraní určujú funkcionalitu PSCs.

Cieľom tejto práce je štúdium vplyvu zabudovania uhlíkových nanobodiek (CNDs v PCBM eletrónovej trasportnej vrstve invertovaných solárnych článkov na ich vlastnosti. Ukázali sme, že zabudovanie CNDs v PCBM zvýši konverziu účinnosti o 12% pre koncentráciu dopovania 1 w% CNDs. Naviac, pozorovali sme zvýšenie krátkodobej stability dopovaných PSCs. Toto pozoruhodné zvýšenie stability môže byť vysvetlené pasivačným efektom CNDs, menovite zapĺňaním pascí vytvorených fotodimerizáciou a fotoionizáciou PCBM molekúl eletrónmi.

V druhej časti tejto práce je študovaný efekt rôznych typov zapuzdrenia PSCs s použitím adhezívnych polymérov alebo Al_2O_3 vrstvou nanesenou vrstvovou depozíciou atómov (ALD). Ukázali sme, že vrstva zapuzdrenia Al_2O_3 hrubá 25 mm a deponovaná pri teplotee 50° C metódou ALD je efektívnou bariérou pre difúziu vlhkosti a významne potláča degradačné procesy v PSCs počas 4000 hodín.

Abstract

Perovskite solar cells (PSCs) revealed impressive progress in power conversion efficiency (PCE) from 9 % up to 25% during the last 10 years. PSCs are multilayers, where the active perovskite layer is placed between the layers for selective charge transport to electrodes. Structure, morphology and transport properties of the layers and interfaces determine the performance of PSCs.

The aim of this work is to study the effect of incorporation of carbon nanodots (CNDs) in the PCBM electron transport layer of the inverted planar PSCs on their performance. It is shown that the incorporation of carbon nanodots in the PCBM results in an increase of the PCE by 12% for the doping concentration of 1 wt% of CNDs. Additionally, increased short term stability of the doped PSCs was observed. The remarkable improvement of the short-term stability could be explained by the passivation effect of CNDs, namely electron filling the traps formed by the photo-dimerization and photo-oxidation of PCBM molecules.

In the second part of this thesis the effect of different type of encapsulation by adhesive polymer and/or by Al_2O_3 atomic layer deposition (ALD) is studied. It is shown that the 25 nm thick encapsulation layer of Al_2O_3 deposited by low temperature ALD (50°C) is an effective barrier against moisture diffusion and significantly suppress the degradation processes in the PSCs for 4000 hours.

1. Introduction

The hybrid organic-inorganic perovskite solar cells (PSCs) have attracted much attention due to their impressive progress in the power conversion efficiency (*PCE*) exceeding at present 22% [1–3]. This high value of *PCE* of PSCs is mainly attributed to a strong optical absorption, low exciton binding energy, long free carrier diffusion length and unique defect tolerance of the organic-inorganic hybrid perovskite materials[4–6]. The key parts of the PSCs are the active perovskite layer converting light into electric charges and the electron and hole transport layers that transfer the respective charge carriers to the electrodes. Structure, morphology and transport properties of the layers and interfaces determine the performance of PSCs[7–9].

The direct (transparent electrode/ETL/PERO/HTL/metal electrode) and inverted (transparent electrode/HTL/PERO/ETL/metal electrode) devices are prepared. The high quality of the perovskite layer, its morphology and crystallinity, proper design of the ETL and HTL and interfaces chemistry and morphology are the crucial factors to efficiently transport the photocarriers to the selective contacts. The stability of the PSC device is at present the most important issue affecting the wide application of the PSCs devices. The degradation mechanisms are influenced by the perovskite surface cations and surface termination groups and also by the degradation processes in ETL and HTL[10–12] .

In my thesis, I focused on the study of the effect of incorporation of carbon nanodots (CNDs) in the PCBM electron transport layer of the inverted planar PSCs on their performance. It is shown that the incorporation of carbon nanodots in the PCBM results in an increase of the PCE by 12% for the doping concentration of 1 wt% of CNDs. Additionally, increased short term stability of the doped PSCs was observed. The remarkable improvement of the short-term stability could be explained by the passivation effect of CNDs, namely electron filling the traps formed by the photo-dimerization and photo-oxidation of PCBM molecules.

In the second part of the thesis the effect of different type of encapsulation by adhesive polymer and/or by Al_2O_3 atomic layer deposition (ALD) is studied. It is observed that the water resistance and thermal stability of the organic-inorganic perovskite layer can be significantly improved by the adhesive PI tape encapsulation. The results revealed that the encapsulated $MAPbI_3$ based films could retain tetragonal perovskite crystal structure at 240°C for more than 180 mins in the ambient environment. The stable operation of encapsulated PSCs in DI water with a power conversion efficiency (PCE) of 19.1% was achieved, which was slightly higher than that

of the device in air (18.2%). Also it is shown that the 25 nm thick encapsulation layer of Al_2O_3 deposited by low temperature ALD (50°C) is an effective barrier against moisture diffusion and significantly suppress the degradation processes in the PSCs for 4000 hours.

2. Aim of the work

The aim of the thesis is to study the effect of incorporation of carbon nanodots in the ETL of the inverted PSCs and to investigate the effect of encapsulation techniques (ahesive polymer, Al_2O_3 ALD layer on the long term stability of the PSCs.

The particular goals are:

1. To master the preparation of the inverted PSCs (p-i-n) with $MAPI_3$ perovskite layer and PSS:PEDOT and PCBM charge transport layers;
2. To optimize the the antisolvent engineering procedure applied for perovskite layer in order to induce heterogenous nucleation of the perovskite. To compare the effect of ambient on the preparation of PSCs (clean room with controlled humidity) .
3. To master the preparation of the n-i-p planar PSCs with $MAPI_3$ perovskite with SnO_2 layer composed of SnO_2 nanoparticles as ETL and spiro –MeOTAD HTL.
4. To study the effect of the modification of ETL in inverted perovskite solar cell by incorporation of the carbon nano dots:
5. To study the effect of advanced encapsulation techniques to the PSCs on the long-term stabilty.

The tasks 1-4 were performed at the IP SAS. The encapsulation studies were performed in collaboration with the Institute of Advanced Materials and Technology, University of Science and Technology Beijing, China (adhesive polymers) and Institute of Electrical Engineering SAS (ALD deposition).

3. Analytical techniques used

The AFM technique measures the morphology of the sample surface by evaluating the forces acting between the vibrating probe and surface. The dimensions of the probing tip limit the AFM resolution. Within today's technology, the sharpness of the scanning tip can be less than a few nanometers. We have used AFM techniques to analyses the morphology of the different layers used to fabricate the PSCs especially the $CH_3NH_3PbI_3$ layer.

Profilometer is an instrument used to evaluate roughness and thickness of the surfaces. A cantilever that scans the surface at a certain speed performs the measurement. The deflection of the tip due to difference in thickness is recorded. In this thesis, the profilometer used is a Dektak Veeco 150.

The resolution limit of the optical microscope can be surpassed by decreasing the wavelength of the light. The electron microscopes use this fact, and instead of the visible light, they use electrons as the probing particles. The microscope resolution is given by the de Broglie wavelength of used electrons, and hence the atomic resolution can be achieved. The transmission electron microscope (TEM) uses electromagnetic lenses to create a magnified image of a thin sample on a two-dimensional detector.

The Energy Resolved Electrochemical Impedance Spectroscopy (ER-EIS) method consists in the application of electrochemical oxidation-reduction contact that provides straightforward information on the density of states at the position of electrochemical potential of the electrolyte, adjustable by the external voltage in a wide range of energies (up to 6 eV) inaccessible by other methods. Perovskite layers deposited on ITO/glass substrate were measured using the three-electrode electrochemical cell. The redox reactions taking place among the gap states at the perovskite/electrolyte interface. Voltage window of the used electrolyte allows to map localized DOS acting as redox centres in the range of ±3V with corresponds to Ag/AgCl reference electrode, which covers most of band gaps of all organic semiconductors.

The Kelvin Probe is a non-destructive technique to measure the work function of the sample surface. It is function as on a vibrating capacitor with interact with the sample surface and measures the work function. In the case of non-metals, the work function is measured the surface potential between the conducting specimen and the vibrating tip.

The X-ray photoelectron spectroscopy (XPS) was used to analyze the atomic composition of samples. The XPS analyzes the kinetic energy of photoelectrons emitted from the sample surface after the absorption of X-ray photons. The binding energy can be determined as the difference between the X-ray photon energy and the kinetic energy of emitted photoelectrons.

The external quantum efficiency (EQE) is an important measurement because correlate the efficiency to the wavelength. In fact, the EQE evaluates the ratio between the incident photons and the electrons extracted for every wavelength. A light source, a xenon lamp, a monochromatic and a source meter, connected to a computer (SpeQuest), compose the system.

The most significant measurement for a PSC is the J-V characteristic under solar illumination condition, which is provided by a solar simulator (Fig. 4.2). The spectrum and amount of solar energy that arrive the ground is related to the latitude, since higher is the latitude, more is the air mass that the light should pass through. For this reason, ASTM has defined some standard to have a correct comparison: Air Mass 0 (AM 0), corresponding to the radiation just outside the atmosphere, data important for instance for satellite, Air Mass 1 (AM 1), indicate the radiation on the Earth with sun in zenith and Air Mass 1.5 (AM 1.5), indicate radiation hitting the surface at a latitude of 48.2.

4. Results *(Part- 1)*

4.1 Development of the p-i-n an n-i-p planar PSCs with anti-solvent method

In order to control the morphology and kinetics of the crystal growth of the perovskite layer the anti-solvent method was introduced by Jeon et al.[13]. In this method, the precursor components are mixed in the polar solvent and then a drop a non-polar solvent is added during spin coating, which induces the heterogeneous nucleation of the perovskite. The optimum timing and amount of the dropping solvent is important for the quality perovskite layer. Fig. 1.1 depict the SEM image of the $MAPbI_3$ layer prepared using anti-solvent engineering. The charge trasnport layers of the PSCs were also prepared by spincoating and thermal treatment. The process was adjusted according to our laboratory conditions to obtain the PSCs with good performance.

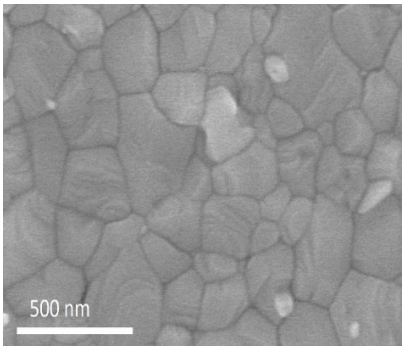

(a)

Figure 1.1 High magnification SEM image of (a) ITO/PEDOT:PSS/perovskite layer prepared by antisolvent engineering.

Fig. 1.2 a,b represents the XRD pattern of the PSCs device and $CH_3NH_3PbI_3$ layer deposited on FTO/SnO_2 substrate respectively. The perovskite layer in both cases were prepared using anti-solvent method. The type of substrate did not affect the crystalline structure of the perovskite layer. It is identified as tetragonal structure with main peaks appeared at 14.12°, 31.86°, 40.45° with the corresponding (310), (224), (314) planes[14,15]. It indicates that the perovskite crystal growth in ITO/PEDOT:PSS and FTO/SnO_2 substrates are identical.

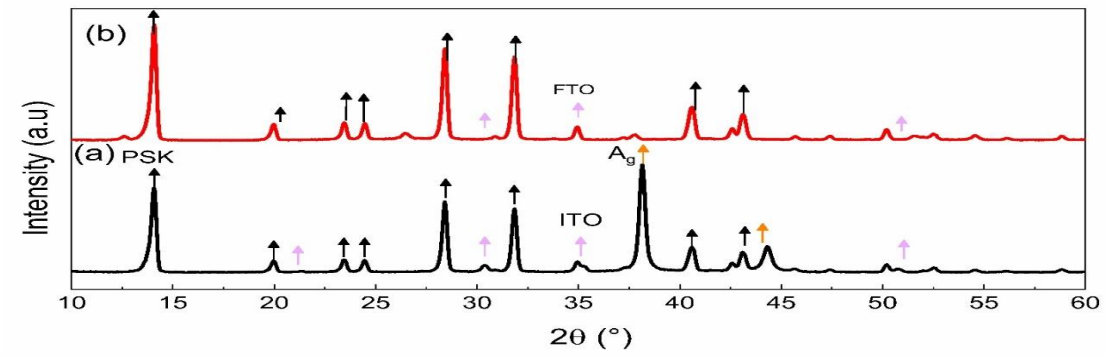

Figure 1.2 XRD pattern of the inverted (a) and part of direct (b) device.
(a) ITO/PSS: PEDOT/$CH_3NH_3PbI_3$/PCBM/Bcp/Ag
(b) FTO/SnO_2/ $CH_3NH_3PbI_3$

We have elaborated the preparation of planar p-i-n (inverted) and n-i-p (direct) PSCs the following stack of layers ITO/PSS:PEDOT/$CH_3NH_3PbI_3$/PCBM/Bcp/Ag and FTO/SnO_2/$CH_3NH_3PbI_3$/Spiro-MeOTAD/Ag in our laboratory. The prepared PSCs have been characterised by J/V characteristics measurements using the class A sun simulator (ABET, AM 1.5).

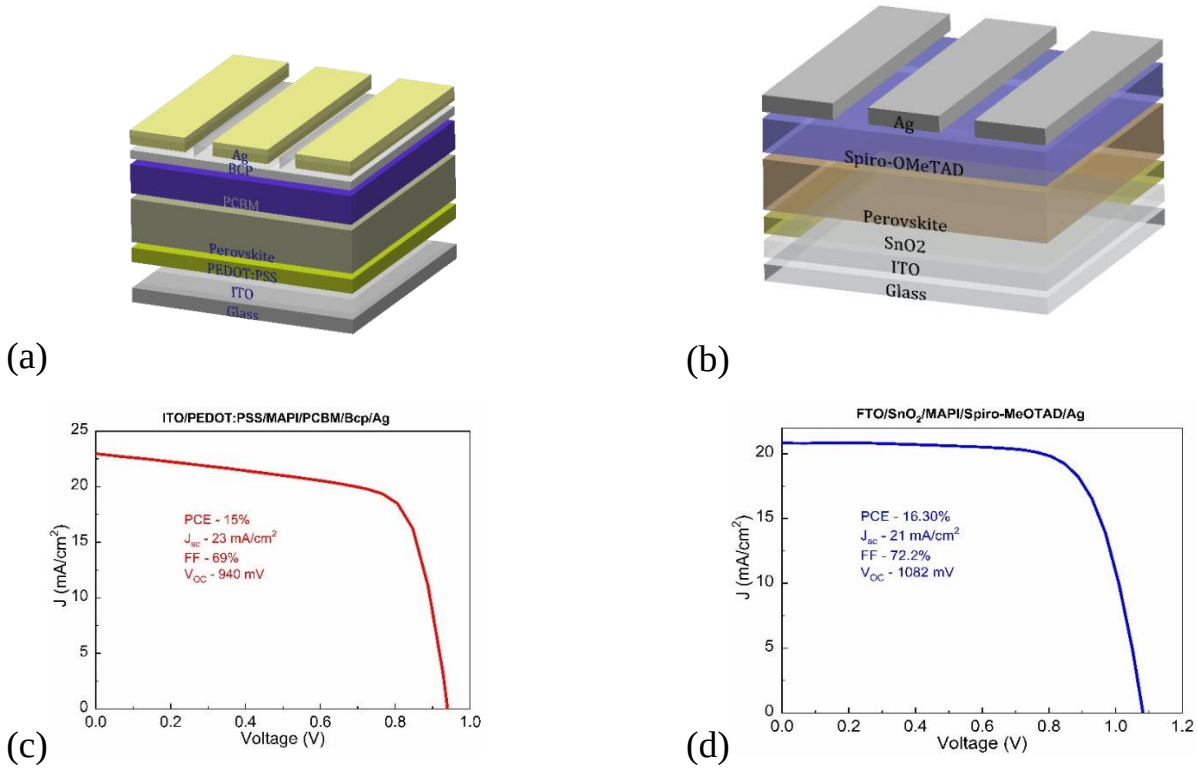

Figure 1.3 Schematic structure of the (a) p-i-n PSCs (b) n-i-p PSCs and *I-V* characteristics of the best PSCs (d) p-i-n PSCs (d) n-i-p PSCs.

We have achieved PCE of 15% (short circuit current J_{sc} – 23 mA/cm^2, fill factor FF – 69%, open circuit voltage V_{oc} – 940 mV) in inverted planar PSCs with PEDOT: PSS as HTL (Fig. 1.3c) and which is comparable with the PCEs currently reported for the same structure. The achieved reproducibility of the PSCs allowed reliable studies of various effects. In the n-i-p PSCs we have achieved PCE 16.30% (J_{sc} – 21mA/cm^2, FF – 72.2%, V_{oc} – 1082 mV) with solution processed SnO_2 as ETL (Fig. 1.3d).

4.2 Doping of $PC_{61}BM$ electron transport layer with carbon nanodots (CNDs) in inverted planar $MAPbI_3$ perovskite solar cells.

The doping effect of carbon nanodots in the $PC_{61}BM$ electron-transport layer on the performance of inverted planar $MAPbI_3$ perovskite solar cells (PSCs) having two different kinds of the hole-transport layer, namely organic PEDOT:PSS and inorganic NiO_x, was investigated. In this work, the effect of the $PC_{61}BM$ layer doping with carbon nanodots (CNDs) up to 3 wt.% on the performance of inverted planar PSCs is studied. Two types of PSCs with different HTL were fabricated, namely ITO/NiO_x/$MAPbI_3$/$PC_{61}BM$/BCP/Ag and ITO/PEDOT:PSS/$MAPbI_3$/$PC_{61}BM$/BCP/Ag. The *J-V* characteristics, external quantum efficiency (*EQE*) and electrical conductivity measurements were complemented by the density of states (DOS) mapping by the energy-resolved impedance spectroscopy (ER-EIS) [16] of a $PC_{61}BM$ layer with the same doping to elucidate the effect of CNDs on *PCE.*

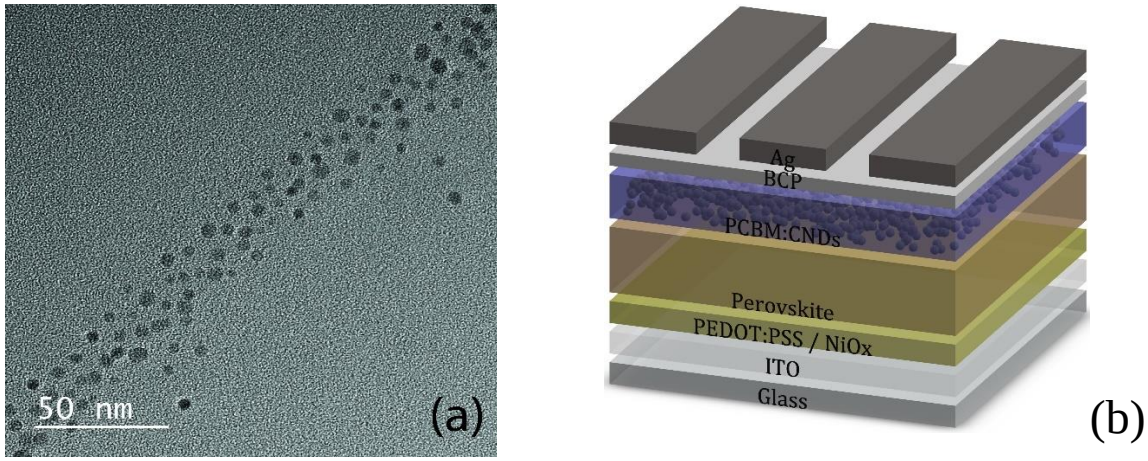

Figure 1.4 (a) HRTEM image of CNDs (b) Schematic device structure of the PSCs doped with CNDs.

The high-resolution transmission electron microscopy (HRTEM) image of the CNDs (Fig. 1.4a) shows the particles of spherical shape with a diameter of 5 ± 0.95 nm. Fig. 1.4b depicts the schematic device structure of the PSCs with doped ETL with CNDs.

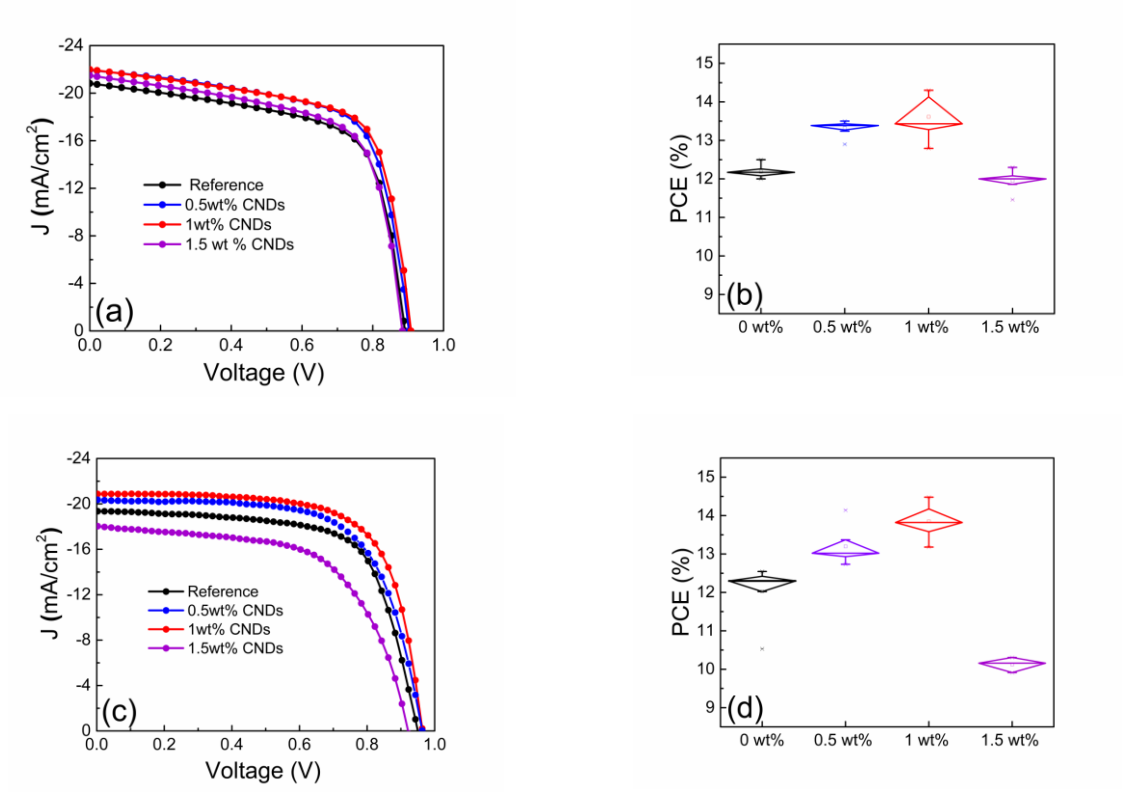

Figure 1.5 (a) Typical *J-V* curves under illumination and (b) PCE statistics of the PSCs (PEDOT:PSS) devices. (c) Typical *J-V* curves under illumination and (d) *PCE* statistics of the PSCs (NiO_x) devices. The $PC_{61}BM$ layer was doped with 0-1.5 wt. % CNDs. The statistics was done over 10 devices for each doping concentration except for 1.5 wt. % CNDs where 5 devices were used.

Table 1. Average photovoltaic parameters of the PSCs (NiO_x) and PSCs (PEDOT:PSS) devices with the 0-1.5 wt.% CNDs doping of the $PC_{61}BM$ layer.

ITO/NiO_x/$MAPbI_3$/$PC_{61}BM$:CNDs/BCP/Ag				
CNDs concentration (wt.%)	J_{sc} (mA/cm^2)	V_{oc} (V)	*FF* (%)	*PCE* (%)
0 (Reference)	19.8	0.95	66.1	12.4
0.5	20.5	0.97	66.4	13.2
1.0	21.2	0.97	67.0	13.8
1.5	18.2	0.92	60.3	10.1
ITO/PEDOT:PSS/$MAPbI_3$/$PC_{61}BM$:CNDs/BCP/Ag				
0 (Reference)	20.8	0.89	65.2	12.1
0.5	21.9	0.90	66.7	13.1
1.0	21.9	0.91	67.2	13.4
1.5	21.4	0.88	64.6	12.2

The effect of the $PC_{61}BM$ doping with CNDs on the current density–voltage (*J-V*) characteristics under illumination for both kinds of PSCs is shown in Figs. 1.5a, c. The devices with undoped PCBM display a 12.4% average efficiency with NiO_x as HTL and 12.1% when employing PEDOT:PSS. These values are in line with p-i-n perovskite solar cells with $CH_3NH_3PbI_3$ processed in air [17]. The photovoltaic parameters derived from *J-V* curves are summarized in Table 1. The maximum improvement of all photovoltaic parameters is obtained for the $PC_{61}BM$ doping with 1 wt.% CNDs. For the PSCs (PEDOT:PSS) devices, the- *PCE* increased by ~11% on average and by 18% at maximum. For the PSCs (NiO_x) devices, the *PCE* increased by ~12% on average and by 16% at maximum.

The high electron density of CNDs increases three times the electrical conductivity of the doped $PC_{61}BM$ layer, which is beneficial for the electron collection. Simultaneously, the V_{oc} increase point to a reduction in surface recombination at the perovskite/ETL interface. Moreover, additional free-charge carriers detected by the ER-EIS method via the polaron states in the band gap are generated in the $PC_{61}BM$ layer under illumination with positive effect on J_{sc}. Such an active role of the $PC_{61}BM$ layer in the PCE improvement has not yet been addressed.

For practical applications, stability issue may be even more important than the absolute *PCE* value. Stability studies of the PSC (PEDOT:PSS) device under a continuous 24-hour 1.5 AM illumination revealed a nearly five times smaller final *PCE* decrease for the 1 wt.% CNDs doping comparing to the undoped counterpart. The favorable effect of CNDs might come from filling the traps formed by the photo-dimerization and photo-oxidation of $PC_{61}BM$ molecules. The passivation of the traps at the perovskite/ETL interface by CNDs, which is manifested by V_{oc} increase, is another favorable factor contributing to the remarkably improved short-term stability of the PSC.

The passivation effect comes from the high electron density typical for carbon materials such as CNDs. It has been also shown that n-doping of $PC_{61}BM$ such as that with CNDs may improve surface wettability of $PC_{61}BM$ when being spin coated on the perovskite layer which results in fewer voids and other non-radiative defects at the perovskite/$PC_{61}BM$ interface. Another mechanism leading to an improvement of the PSC performance can be connected with mobile ionic species associated with vacancies, ions, or interstitial defects[20]. The migration of such mobile ions causes band bending due to the electric field screening effect or a change of the local doping with impact on the charge extraction efficiency. The internal electric field due to the work

function difference between ETL and HTL drives the migration of the positively charged point defects (e.g. iodide vacancy, methylammonium iodide interstitial) toward the HTL, while the negatively charged point defects (e.g. methylammonium iodide vacancy, iodide interstitial) migrate in the opposite direction in dark [21]. The accumulation of these charged ions at the perovskite interface with ETL and HTL creates an additional electric field across the perovskite film that is opposite to the internal electric field and decreases the photogenerated charge collection. The high electron density of CNDs in the PCBM can act beneficially against such ion migration and contribute to enhanced solar cell parameters and improved temporal stability (see Fig. 1.6).

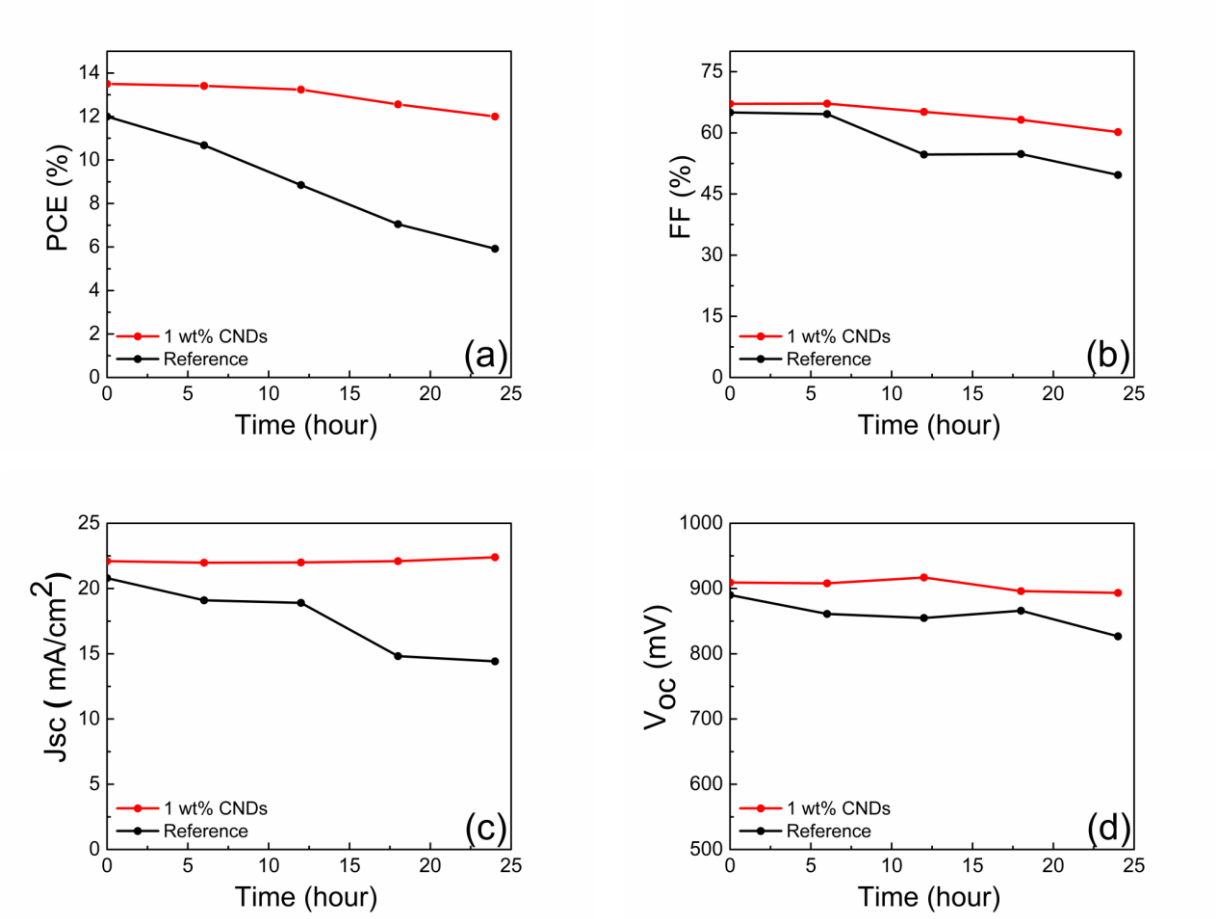

Figure 1.6. Temporal evolution of the photovoltaic parameters of the PSCs (PEDOT:PSS) devices with the undoped $PC_{61}BM$ layer and after the doping with 1 wt.% CNDs under continuous AM 1.5 illumination in air (~40% humidity) – (a) *PCE*,(b) *FF*, (c) J_{sc};(d)V_{oc}.

The stability study results show (Fig. 1.6) that the doping of the $PC_{61}BM$ layer with 1 wt.% CNDs results in a significant short-term stability increase of the PSCs (PEDOT:PSS) device. There are several factors which could explain this improvement. The photo-dimerization of $PC_{61}BM$ molecules under light exposure resulting in the formation of shallow traps and a decrease of the charge carriers mobility was reported [22]. It was also shown that photo-dimerization in fullerenes is directly linked to J_{sc} losses in organic solar cells [23]. In this regard, it is worth noting that J_{sc} exhibits the biggest relative decrease in the PSC with the undoped $PC_{61}BM$ layer comparing to *FF* and V_{oc} (Fig. 1.6c). This suggests that photo-dimerization of $PC_{61}BM$ molecules is one of the main factors responsible for the PCE degradation observed in the undoped PSC [23,24]. The high electron density of CNDs in the doped device could slow down this process by electron filling the traps induced by photo-dimerization. The photo-oxidation of $PC_{61}BM$ is another important mechanism affecting stability of the solar cells containing $PC_{61}BM$.

Part- 2 Application of advanced encapsulation techniques for PSCs

4.3 Significant Stability Enhancement of Perovskite Solar Cells by Facile Adhesive Encapsulation.

Facile adhesive encapsulation strategy was employed to improve the stability of perovskite films and PSC devices using the commercial Kapton polyimide (PI) tape. This work was done with the collaboration of Institute of Advanced Materials and Technology, University of Science and Technology Beijing, China. We investigated the perovskite films and PSCs in extreme conditions (in DI water or under thermal treatment at 85°C or 240°C). The results revealed that the encapsulated $MAPbI_3$ based films could retain tetragonal perovskite crystal structure at 240°C for more than 180 mins in the ambient environment. The stable operation of encapsulated PSCs in DI water with a power conversion efficiency (PCE) of 19.1% was achieved, which was slightly higher than that of the device in air (18.2%). This study demonstrated the improvement of stabilities was correlated with the adhesion force between encapsulation film and the surface of perovskite film.

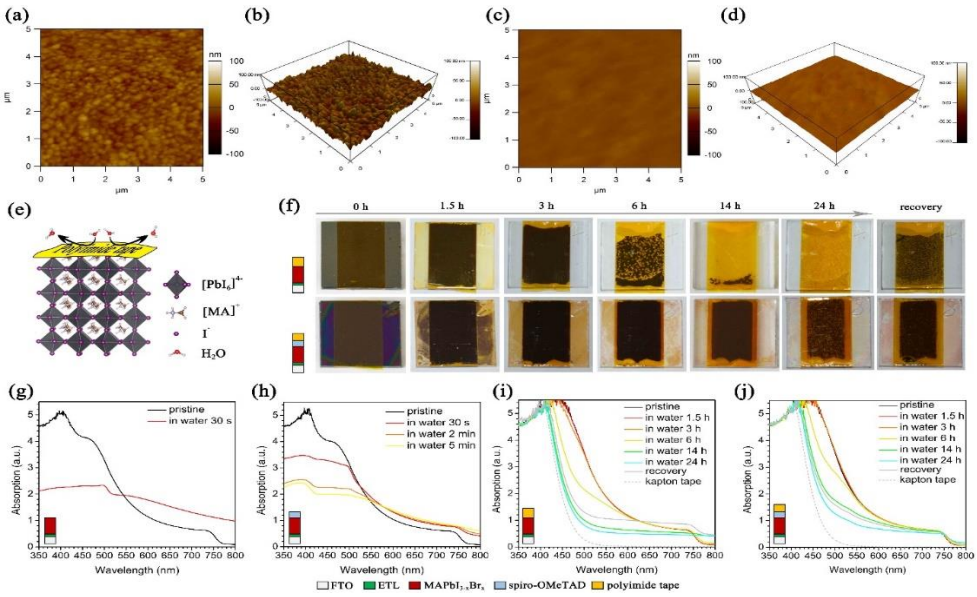

Figure 1.7. Topography and three-dimensional AFM images of $MAPbI_{(3-x)}Br_x$ perovskite film (a, b) and $MAPbI_{(3-x)}Br_x$/spiro-OMeTAD film (c, d); (e) schematic illustrations of the elimination of the potential diffusion path of ambient water molecule into perovskite structure; (f) optical images of $MAPbI_{(3-x)}Br_x$ perovskite films and $MAPbI_{(3-x)}Br_x$/spiro-OMeTAD films with encapsulation after immersion in water for different period of time; ex situ UV-vis absorption spectra of perovskite film (g), perovskite/spiro-OMeTAD film (h), perovskite/PI tape film (i) and perovskite/spiro-OMeTAD/PI tape film (j) after immersion in DI water for different time.

To verify the water resistance of the perovskite films with adhesive encapsulation, we performed UV-vis absorption measurements for the perovskite films immersed in DI water. In Figure 1.7 (g-j), we show the ex situ UV-Vis absorption spectra of $MAPbI_{(3-x)}Br_x$ perovskite and $MAPbI_{(3-x)}Br_x$/spiro-OMeTAD films without and with encapsulation for different immersion period of time. In the spectrum taken after immersing in water for non-encapsulated perovskite films, the characteristic absorption edge of $MAPbI_{(3-x)}Br_x$ perovskite around 775 nm disappears, while the characteristic absorption edge around 539 nm is corresponding to the decomposition products PbI_2. For the unencapsulated $MAPbI_3$/spiro-OMeTAD films, the water degradation kinetics is slowed down due to the protective action of spiro-OMeTAD. However, the PbI_2 absorption feature is also observed after immersion for 30 s. The reduced absorbance at short wavelength region and obvious light scattering at long wavelength region indicate the deterioration

of perovskite morphology, which implies that the H_2O molecule will infiltrate through the spiro-OMeTAD layer to degrade perovskite. The UV-vis absorption spectra show no visible changes for the encapsulated $MAPbI_{(3-x)}Br_x$ perovskite films after immersion in water for 1.5 h, and it further prolongs to 3h for the encapsulated $MAPbI_{(3-x)}Br_x$/spiro-OMeTAD films. Besides, the characteristic absorption edge of perovskite for encapsulated $MAPbI_{(3-x)}Br_x$/spiro-OMeTAD films changes little during the measurement. These results confirm that the excellent water resistance of perovskite films is achieved by the adhesion encapsulation.

We investigated the stable power output at the maximum power point (MPP) of PSCs devices immersed in water under continuous AM 1.5 irradiation. The loss of stabilized PCE is comparable for both the unencapsulated and encapsulated PSCs devices measured in air condition within 150 s (from 30 s to 180 s). Then we poured the DI water to immerse the devices during the measurements. We also observed 5~6% improvement of stabilized efficiency in DI water due to the light refraction effect. The stabilized PCE of unencapsulated device rapidly drops to 0% in water for 293 s, while it prolongs to 1522 s for the device encapsulated by one layer of PI tape, the PSCs device encapsulated by two layers PI tape maintains 89.3% of its initial efficiency after immersion in water for 1620 s (from 180 s to 1800 s).

The stabilized efficiency of PSCs device based on planar SnO_2 architecture retains 96.3% of its initial efficiency in water under the same test conditions comparable loss of stabilized efficiency measured in ambient conditions (retains 98.9% of its initial efficiency was observed. These results confirm that the stability of PSCs devices, including mesoscopic and planar structures, is significantly improved by the adhesive encapsulation strategy.

4.4 Low-Temperature atomic layer deposited Al_2O_3 encapsulation for enhanced long-term stability of inverted planar Perovskite Solar Cells.

In this study, low temperature (50° C) ALD technique was utilized to implement pinhole-free Al_2O_3 layers as encapsulation of an inverted perovskite solar cell consisting of ITO/PEDOT: PSS/$CH_3NH_3PbI_3$/$PC_{61}BM$/Bcp/Ag. In order to investigate the long-term stability of PSCs, we used three different thicknesses 10nm, 25nm and 50nm respectively of ALD Al_2O_3. We studied the device performances and the stability in ambient air and high humidity (>40%), with and without encapsulation for 4000 hours. The degradation study of PSCs for such a long term is not often reported in the recent years especially for inverted planar structure. The *J-V* characteristic, external quantum efficiency, XPS elemental depth profile, contact angle measurements and XRD measurements are performed in the encapsulated and non-encapsulated PSCs to analyze the degradation effect and the mechanisms involved.

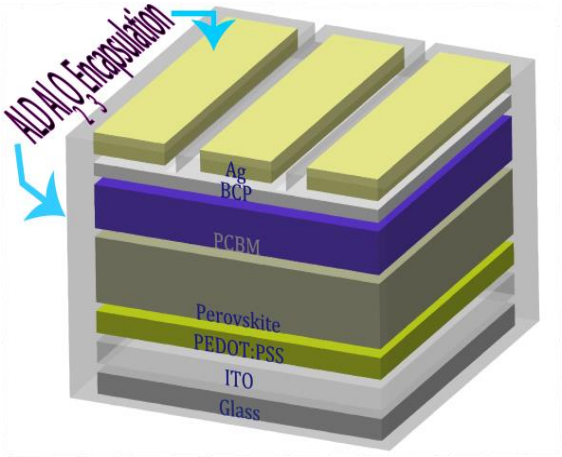

Figure 1.9 (a) schematic device architecture of the encapsulated PSCs

In order to study the degradation of devices by means of their photovoltaics performance, we have chosen a set of devices having close values of PCE. These devices were encapsulated with ALD Al_2O_3 films (Fig. 1.9) with the thickness of 10 nm, 25 nm and 50 nm and the device performances were compared with non-encapsulated pristine PSCs. The *J-V* sweep measurements were done intermittently for 4000 hours for all the devices. Fig. 2.1 depicts the data of the PCE of pristine device together for the encapsulated devices with different ALD Al_2O_3 film thickness. It

apparently shows the Al_2O_3 encapsulation considerably improved the stability of the device compared to the pristine non-encapsulated PSCs. The non-encapsulated devices were degraded completely after 2000 hours, while the encapsulated devices showed low rate of degradation. Table 10.1. Indicates the different average percentages of degradation of devices with and without encapsulation. We observed that the non-encapsulated devices degraded by 43.2 % after 1000 hours while the encapsulated devices by 22.2%, 13.1% and 17.7% degradation with 10 nm, 25 nm and 50 nm respectively.

After 1500 hours exposing in ambient air, the non-capsulated devices were degraded by 53.1% while the encapsulated PSCs showed only 23%, 14.5% and 23.7% with Al_2O_3 encapsulation of 10nm, 25nm and 50nm respectively. Until the 1500 hours we have observed a gradual degradation of non-encapsulated devices even the degradation rate was comparatively high with the encapsulated cells. From 1500-2000 hours, the performance of the non-encapsulated PSCs falls sharply and degraded by 96.9% while the encapsulated PSCs had degradation of 25.2%, 15.5% and 32.4 % with 10 nm, 25 nm and 50 nm Al_2O_3 encapsulation respectively.

More importantly after 4000 hours, the encapsulated PSCs had degraded only by 51.3%, 25.9% and 37% with 10 nm, 25 nm and 50 nm Al_2O_3 encapsulation, respectively. We have observed the comparatively higher degradation in the case of encapsulation with 10 nm thick Al_2O_3 layer in comparison to the thicker encapsulation layers (25 nm and 50 nm). This effect could be related to the possible defects formation in the Al_2O_3 layer enabling the moisture diffusion at very slow rate through the Al_2O_3, which can form H-bonds with oxygen in the surface and the intrinsic oxygen inside the film[25].

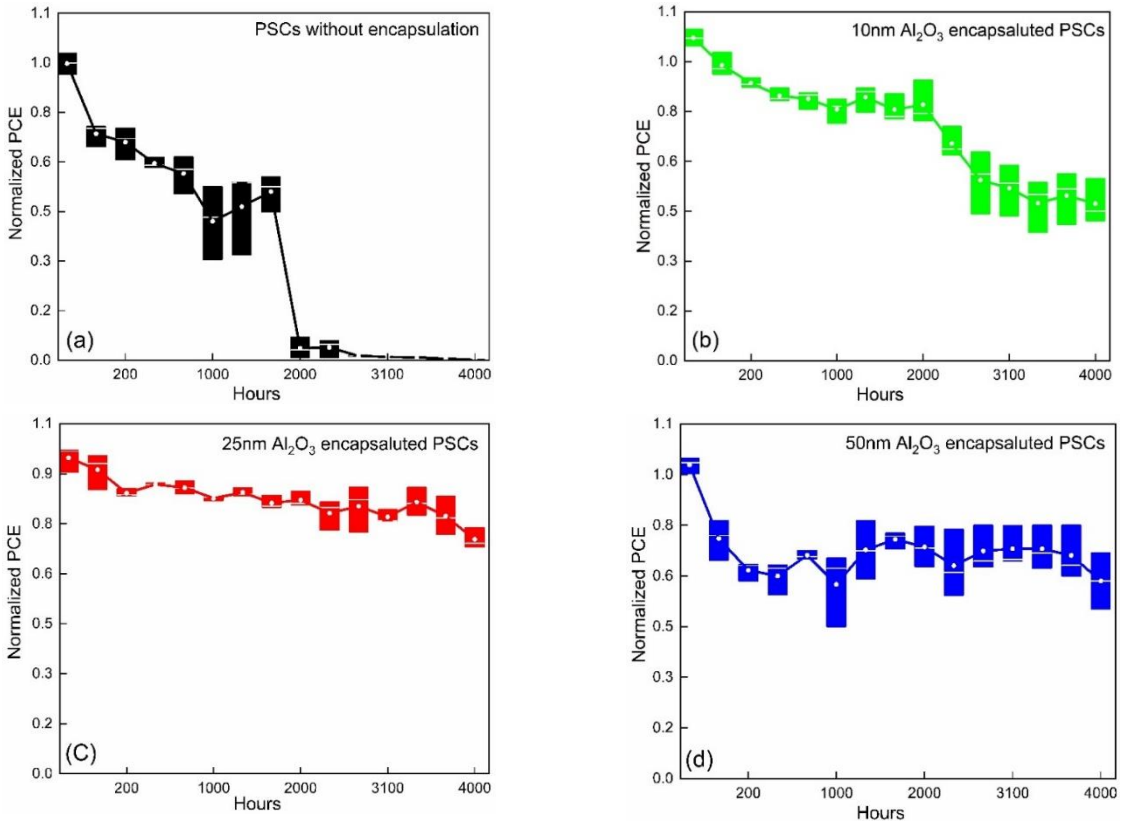

Figure 2.1. Statistical degradation of PSCs PCE of the (a) Fresh pristine PSCs (b) 10 nm (c) 25nm and (d) ALD-Al_2O_3 Encapsulated PSCs.

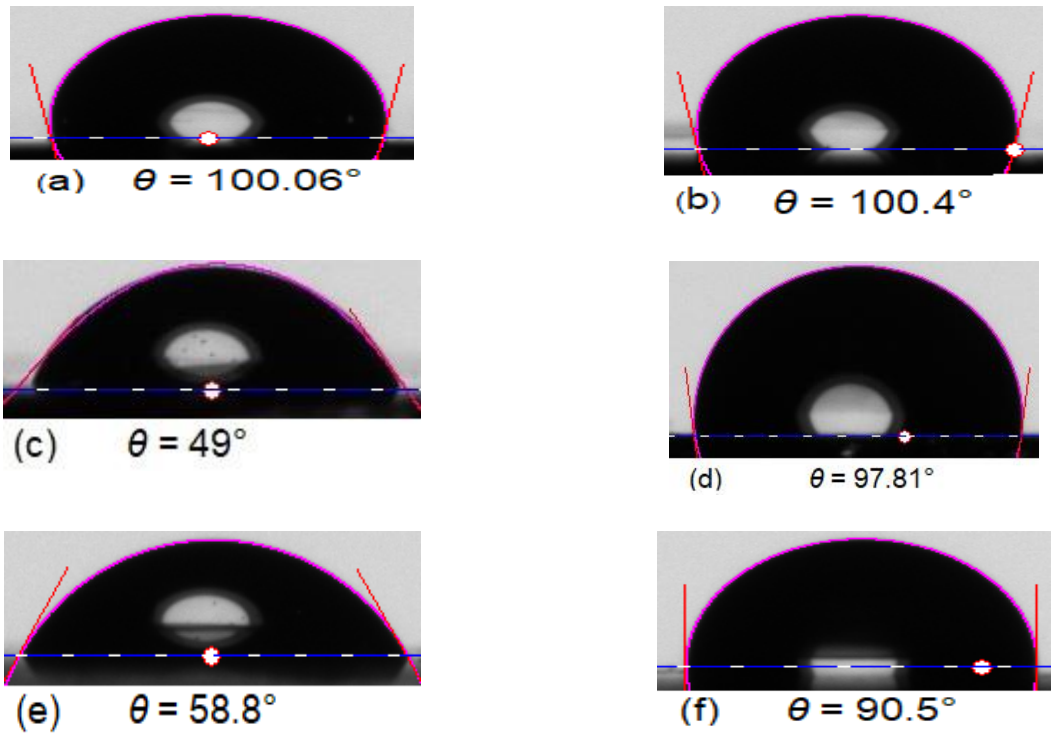

Figure 2.2. Contact angle measuremnents of the non (a) zero sec(c) after 2 mins (e) after 4000 hou zero sec non encapsulated PSCs and (b) Zero sec (d) after 2 mins (f) after 2 mins 4000 hou encapsulated PSCs.

Fig. 2.2 depicts the contact angle measurements of the non-encapsulated and encapsulated devices. We have dropped 5 µl water drop on the top of the both devices, so the water was in contact of the non-encapsulated device ITO/PEDOT: PSS/$CH_3NH_3PbI_3$/$PC_{61}BM$/Bcp and the encapsulated device was ITO/PEDOT: PSS/$CH_3NH_3PbI_3$/$PC_{61}BM$/Bcp/Al_2O_3. After 2 minutes in the non-encapsulated PSCs, we observed a gradual decrease in the contact angle due to the interaction of water with the bcp/PCBM surface. After two minutes, the contact angle was around 49° and the water drop completely diffused into the sample. This is in accordance with the reported water affinity of the PCBM[25]. In the case of encapsulated devices, the hydrophobicity was stable with a very small decrease by 2.5° after 2 minutes. For samples exposed 4000 hours to ambient.

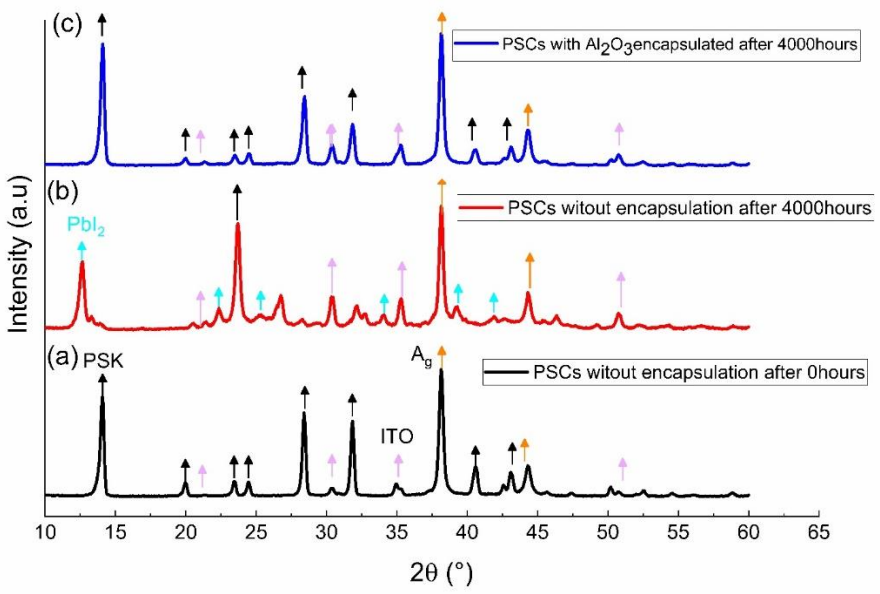

Figure 2.3. XRD pattern of (a) fresh reference device, (b) non encapsulated device after 4000hours and (c) 25nm Al_2O_3 encapsulated devices after 4000hours

We have studied the structural changes of the devices after 4000 hours of degradation in ambient condition by XRD. Fig. 2.3 a represents the different XRD pattern of the fresh device with crystalline structure of $CH_3NH_3PbI_3$. It is identified as tetragonal structure with main peaks appeared at 14.12°, 31.86°, 40.45° with the corresponding (310), (224), (314) planes. In the case of non-encapsulated devices, XRD peaks of the $CH_3NH_3PbI_3$ completely disappeared after 4000 hours and we observed formation of PbI_2 phase (peak at 12.6° 2 theta and others marked green) (Fig.2.3b). This is another conformation that the $CH_3NH_3PbI_3$ in non-encapsulated devices was completely decomposes by the moisture in the presence of air.

5. Conclusions

This thesis is concerned with the development of the planar perovskite solar cells, and different doping of the electron transfer layer with carbon nanodots to enhance the performance and the long-term stability studies of the prepared devices. We analysed in detail the effect of incorporation of carbon nanodots in the PCBM layer of the p-i-n PSCs and the application of adhesive polymer and an ALD encapsulation technique to enhance the long-term stability of the PSCs. We optimized p-i-n PSCs with PCE over 15% and n-i-p PSCs over 16%. The developed PSCs, different device fabrication techniques and the comparison of the photovoltaics properties are discussed. The effect of the doping of $PC_{61}BM$ electron transport layer with carbon nanodots on the performance of inverted planar $MAPbI_3$ perovskite solar cells having two different HTL namely PEDOT:PSS and solution processed NiO_x was studied. An average 11% and 12% increase of PCE was achieved for 1wt% carbon nanodots doping in the PSCs with PEDOT: PSS and NiO_x respectively. This enhancement corresponds to the high electron density of CNDs. It improved three times the electrical conductivity of the ETL and the passivation mechanism of the $MAPbI_3/PC_{61}BM$ interface become more feasible. This effect is directly observed in the increase of V_{oc}. Also, the parallel resistance and fill factor of the PSCs were enhanced. Moreover, the ER-EIS measurements revealed additional free-charge carriers in the $PC_{61}BM$ layer generated under illumination that were detected via the polaron states formation in the band gap with positive effect on the J_{sc}. All these factors contribute to the improvement in the PCE. Stability tests of the PSC with PEDOT:PSS under a continuous 24 hour 1.5 AM illumination showed a five times smaller final PCE decrease for the 1wt% CNDs doping of the $PC_{61}BM$. The remarkable improvement of the short-term stability could be explained by the passivation effect of CNDs, namely electron filling the traps formed by the photo-dimerization and photo-oxidation of PCBM molecules.

Studies of the facile adhesive encapsulation for stability enhancement of PSCs demostrated that an adhesive encapsulation by employing the commercial polyimide tape can significantly improve the water resistance and thermal stability of $CH_3NH_3PbI_3$ perovskite films and PSCs. The PCE of 19.1% was obtained with the stable operation of encapsulated PSCs in water and PCE of 18.2% was achieved in air. In addition, 96.3% of its initial efficiency in water for 1620 s under continuous illumination was achieved. The tetragonal crystal strucure of $CH_3NH_3PbI_3$ was retained after heated at 240°C for 180 min in an ambient of the encapsulated perovskite film. This adhesive encapsulation offers an avenue to improve the stability of PSCs for future commercialization.

We have elaborated the low-temperature atomic layer deposited Al_2O_3 encapsulation for p-i-n PSCs and enhanced the long-term stability of the devices. We have achieved a significant increment of the operation lifetime of the encapsulated PSCs compared to the non-encapsulated PSCs. The operation lifetime of encapsulated PSC was 74% increased than the non-encapsulated PSCs after 4000 hours in ambient air and high humidity (>40%). The XPS elemental depth profile measurements of the encapsulated and non-encapsulated PSCs reveals that even after 4000 hours of exposure of the encapsulated PSCs in ambient air and such high humidity (<40%) was not caused any significant damage of the interfaces and interlayers of the PSCs. In addition, it is evidently proved that the $CH_3NH_3PbI_3$ in non-encapsulated devices is completely decomposed by the moisture in the presence of air confirmed by XRD measurements. In conclusion, low-temperature (50°C) ALD- Al_2O_3 encapsulation technology is very effective for PSCs long-term stability and can be an important factor for futuristic commercialization of perovskite photovoltaics.

List of author's publications

1. **Riyas Subair**, Diego Di Girolamo, Michal Bodik, Vojtech Nadazdy,BoLi, Peter Nadazdy, Zoran Markovic, Monika Benkovicova, Juraj Chlpikg, Mario Kotlar, Yuriy Halahovets, Peter Siffalovic Matej Jergel, Jianjun Tian, Francesca Brunetti, Eva Majkova "Effect of the doping of $PC_{61}BM$ electron transport layer with carbon nanodots on the performance of inverted planar $MAPbI_3$ perovskite solar cells". *Sol. Energy* **189,** 426–434 (2019).
2. Bo Li, Mengru Wang, **Riyas Subair**, Guozhong Cao, and Jianjun Tian "Significant Stability Enhancement of Perovskite Solar Cells by Facile Adhesive Encapsulation". *J. Phys. Chem. C* **44,** 25260–25267 (2018)
3. Karol Frohlich, Miroslav Mikolášek, **Riyas Subair**, Vojtech Nadazdy, Alica Rosová, Marian Precner, Nevin Tasaltin, Elif Alturk, Emine Tekin, Emre Aslan, Tulin Ates Turkmen, Eva Majková "Application of Atomic Layer Deposition for Fabrication of Solar Cells" meeting abstract,The Electrochemical Society 1144-1144 (2019)
4. Krzysztof Artur Bogdanowicz, Beata Jewłoszewicz, Agnieszka Iwan, Karolina Dysz, Wojciech Przybyl, Adam Januszko, Monika Marzec, Kacper Cichy, Konrad ´Swierczek, Ladislav Kavan, Markéta Zukalová, Vojtech Nadazdy, **Riyas Subair,** Eva Majkova, Matej Micusik, Maria Omastova, Mehmer Derya Özeren, Katalin Kamarás, Do Yeon Heo, and Soo Young Kim "Selected Electrochemical Properties of 4,4'-((1E,1'E)-((1,2,4-Thiadiazole-3,5-diyl)bis(azaneylylidene))bis (methaneylylidene))bis(N,N-di-p-tolylaniline) towards Perovskite Solar Cells with 14.4% Efficiency". *Materials* **3,** 4–17 (2020).
5. **Riyas Subair** , Bijay Prakash Tripathi, Peter Formanek , Frank Simon , Petra Uhlmann , Manfred Stamm "Polydopamine modified membranes with in situ synthesized gold nanoparticles for catalytic and environmental applications". *Chem. Eng. J.* **295,** (2016).
6. Bijay P. Tripathi, Nidhi C. Dubey, **Riyas Subair**, Soumydip Choudhury and Manfred Stamm "Enhanced hydrophilic and antifouling polyacrylonitrile membrane with polydopamine modified silica nanoparticles". *RSC Adv.* **6,** 4448–4457 (2016).

Bibliography

[1] M. Saliba, C.-B. Juan Pablo, W. ChristianM., M. Stolterfoht, N. Phung, S. Albrecht, D. Neher, A. Abate, *Chem. Mater.* **2018**, *30*, 4193.

[2] NREL, Best-research-cell-efficiencies **2020**.

[3] Z. Wu, M. Jiang, Z. Liu, A. Jamshaid, L. K. Ono, Y. Qi, *Adv. Energy Mater.* **2020**, *10*, 1.

[4] X. Wang, G. Lu, M. Zhang, Y. Gao, Y. Liu, L. Zhou, Z. Lin, *Coatings* **2020**, *10*, 31.

[5] P. Gao, M. Grätzel, M. K. Nazeeruddin, *Energy Environ. Sci.* **2014**, *7*, 2448.

[6] X. Dong, X. Fang, M. Lv, B. Lin, S. Zhanga, J. Ding, N. Yuan, *J. Mater. Chem. A* **2015**, *3*, 5360.

[7] M. Firdaus, M. Noh, H. Teh, R. Daik, *J. Mater. Chem. C* **2018**, *6*, 682.

[8] J. Jeng, Y. Chiang, M. Lee, S. Peng, T. Guo, P. Chen, T. Wen, *Adv. Mater.* **2013**, *25*, 3727.

[9] C.-C. Zhang, M. Li, Z.-K. Wang, Y.-R. Jiang, H.-R. Liu, Y.-G. Yang, X.-Y. Gao, H. Ma, *J. Mater. Chem. A* **2017**, *5*, 2572.

[10] Q. Jiang, L. Zhang, H. Wang, X. Yang, J. Meng, H. Liu, Z. Yin, J. Wu, X. Zhang, J. You, *Nat. Energy* **2016**, *2*, 16177.

[11] D. Luo, W. Yang, Z. Wang, A. Sadhanala, Q. Hu, **2018**, *1446*, 1442.

[12] T. Leijtens, G. E. Eperon, S. Pathak, A. Abate, M. M. Lee, H. J. Snaith, *Nat. Commun.* **2013**, *4*, 1.

[13] N. J. Jeon, J. H. Noh, Y. C. Kim, W. S. Yang, S. Ryu, S. Il Seok, *Nat. Mater.* **2014**, *13*, 897.

[14] T. Leijtens, G. E. Eperon, N. K. Noel, S. N. Habisreutinger, A. Petrozza, H. J. Snaith, *Adv. Energy Mater.* **2015**, *1500963*, 1.

[15] W. Yan, H. Rao, C. Wei, Z. Liu, Z. Bian, H. Xin, W. Huang, *Nano Energy* **2017**, *35*, 62.

[16] V. Nádaždy, F. Schauer, K. Gmucová, *Appl. Phys. Lett.* **2014**, *105*, 1.

[17] J. Ciro, R. Betancur, S. Mesa, F. Jaramillo, *Sol. Energy Mater. Sol. Cells* **2017**, *163*, 38.

[18] Z. Wang, D. P. McMeekin, N. Sakai, S. van Reenen, K. Wojciechowski, J. B. Patel, M. B. Johnston, H. J. Snaith, *Adv. Mater.* **2017**, *29*, 1.

[19] W. Tress, M. Yavari, K. Domanski, P. Yadav, B. Niesen, P. Correa, *Energy Environ. Sci.* **2018**, *11*, 151.

[20] C. Eames, J. M. Frost, P. R. F. Barnes, B. C. O. Regan, A. Walsh, M. S. Islam, *Nat. Commun.* **2015**, *7497*, 2.

[21] B. Chen, P. N. Rudd, S. Yang, J. Huang, P. N. Rudd, *Chem socienty Rev.* **2019**.

[22] A. Distler, T. Sauermann, H. Egelhaaf, S. Rodman, D. Waller, K. Cheon, M. Lee, D. M. Guldi, *Adv. energy Mater.* **2013**, *4*, 1300693.

[23] T. Heumueller, W. R. Mateker, A. Distler, U. F. Fritze, R. Cheacharoen, W. H. Nguyen, M. Biele, M. Salvador, M. Von Delius, H. Egelhaaf, D. Mcgehee, *Energy Environ. Sci.* **2016**, *9*, 247.

[24] W. R. Mateker, M. D. McGehee, Progress in Understanding Degradation Mechanisms and Improving Stability in Organic Photovoltaics. *Adv. Mater.* **2017**.

[25] Y. Lv, P. Xu, G. Ren, F. Chen, H. Nan, R. Liu, D. Wang, X. Tan, X. Liu, H. Zhang, Z. Chen, **2018**.